Geometrical and Electronic Structure of Cation Radical Species of Tetraarylanthraquinodimethane: An Intermediate for Unique Electrochromic Behavior

Yusuke Ishigaki,*[a] Reina Fukagawa,[a] Kazuma Sugawara,[a] Takashi Harimoto,[a] and Takanori Suzuki*[a]

[a] Prof. Dr. Y. Ishigaki, Ms. R. Fukagawa, Dr. K. Sugawara, Mr. T. Harimoto, Prof. Dr. T. Suzuki
Department of Chemistry, Faculty of Science
Hokkaido University
N10 W8, North-ward, Sapporo 060-0810, Japan
E-mail: yishigaki@sci.hokudai.ac.jp; tak@sci.hokudai.ac.jp

Supporting information for this article is given via a link at the end of the document.

Abstract: Two tetraarylanthraquinodimethane (Ar4AQD) derivatives having two different aryl groups (aminophenyl and methoxyphenyl) were prepared by sequential dibromomethylation and Suzuki-coupling reactions. X-ray analyses showed that they adopt a folded structure in the neutral state whereas the corresponding dications have a planar anthracene ring, to which diarylmethylium units are perpendicularly attached. Different from Ar4AQD having the same substituents that undergoes facile two-electron transfer during interconversion with the dicationic state, the intermediary cation radical becomes long-lived in the newly prepared unsymmetric derivatives. The electronic and geometric structures of the open-shell intermediates were elucidated through electrochemical and theoretical investigation, with revealing that the cation radicals adopt the twisted geometry like dications. Upon electrolytes of the dications, the twisted cation radicals were involved in the electrochromism whereas their steady-state concentration is negligible in the oxidation process, thus realizing unique tricolor electrochromic behavior with a hysteretic pattern of color change (colorless -> purple -> blue -> colorless).

Introduction

Organic redox systems undergo reversible electron transfer when the resulting charged species are stable enough.[1–5] Charge delocalization and/or formation of additional aromatic ring upon electron transfer are often adopted strategies to stabilize the organic ions.[6–15] Quinodimethanes are the cross-conjugated π-system,[16,17] which are suitable scaffolds to design the reversible redox systems, especially because of the formation of planar π-skeleton with an additional aromatic ring in the corresponding ion radicals and doubly-charged ions.[18–20]

Based on the general consideration shown above, the pentacenequinodimethane-type dication (**I**$^{2+}$) has a quite peculiar structure, in which the two positive charges are located on the one side of the molecular skeleton (Scheme 1a).[21] Compared to the isomeric dication diradical structure (**II**$^{2+2\bullet}$), the charges in **I**$^{2+}$ are less delocalized over the π-skeleton with an anthracene core on the skeleton. The number of Clar sextet in **I**$^{2+}$ is larger than in **II**$^{2+2\bullet}$, which may, if possibly, account for preference of **I**$^{2+}$.

By considering that **II**$^{2+2\bullet}$ consists of two units of the cation radical of redox-active tetraarylanthraquinodimethane[22,23] (**1**), we envisaged that the detailed examination of the geometrical and electronic structure on **1**$^{+\bullet}$ would provide a valuable information to account for the unique structure of **I**$^{2+}$. Since the cation radical **1**$^{+\bullet}$ is a transient species in the cases of symmetric compounds with the same four aryl groups [**1a**: Ar^1 = Ar^2 = 4-$Me_2NC_6H_4$; **1b**: Ar^1 = Ar^2 = 4-O(CH_2CH_2)$_2$NC_6H_4; **1c**: Ar^1 = Ar^2 = 4-MeOC_6H_4] due to successive two-electron (2e) transfer in both oxidation and reduction steps (Scheme 1b), we have designed here the unsymmetric analogues (**1d**,**1e**), in anticipation that the lifetime of the corresponding cation radicals would be extended.

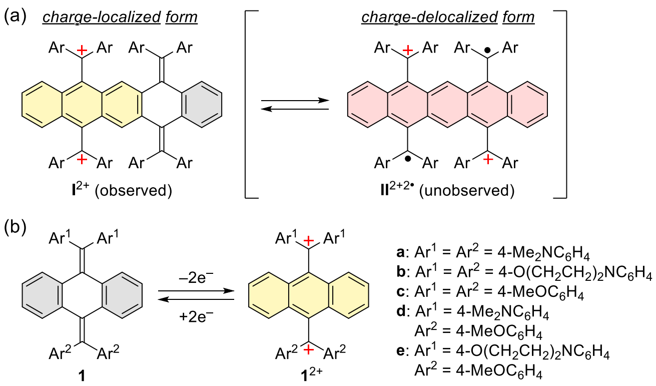

Scheme 1. (a) Charge-localized and -delocalized form (**I**$^{2+}$ and **II**$^{2+2\bullet}$) of extended dications based on bisquinodimethane derivatives. (b) Redox interconversion of anthraquinodimethane derivatives.

We have revealed in this study that **1**$^{+\bullet}$ has a twisted geometry with a planar anthracene ring being attached with a diarylmethylium and a diarylmethyl unit in a perpendicular manner, which is quite different from that of the folded structure of neutral quinodimethane **1**. The geometrical and electronic structure of **1**$^{+\bullet}$ can account for the higher stability of **I**$^{2+}$ than of **II**$^{2+2\bullet}$. The details are disclosed herein.

Results and Discussion

Preparation and molecular geometry of 1d,1e and 1d^{2+},1e^{2+}. The aryl substituents of **1d** (Ar^1 = 4-$Me_2NC_6H_4$, Ar^2 = 4-MeOC_6H_4) are selected so that the 2e-process of **1** to **1**$^{2+}$ or **1**$^{2+}$ to **1** would occur in a stepwise manner by the different electron-donating properties of dimethylamino and methoxy groups as shown by the oxidation peak potential of **1a** (+0.53 V vs SCE in CH_2Cl_2) and **1c** (+1.00 V).[22,24] We also designed **1e** [Ar^1 = 4-O(CH_2CH_2)$_2$NC_6H_4, Ar^2 = 4-MeOC_6H_4] with the expectation that the donating properties of morpholino group are intermediary between the above two (+0.72 V for **1b**).

The symmetric quinodimethanes **1a**-**c** were previously prepared by the quadruple Suzuki-coupling reaction of tetrabromoanthraquinodimethane (**2**) with the corresponding arylboronic acid (Scheme 2a).[22,24] To selectively prepare the unsymmetric derivatives, we adopted the scheme of sequential introduction of aryl groups by using 10-bis(4-methoxyphenyl)methylene-9-anthrone (**4**) as a key synthon. Thus, 10-dibromomethylene-9-anthrone (**3**) was first prepared upon treatment of anthraquinone with CBr_4/P(O*i*Pr)$_3$.[25] The double Suzuki-coupling of **3** with 4-methoxyphenylboronic acid gave **4** in 92% yield. After dibromomethylation of **4** to **5** with CBr_4/Ph_3P, further Suzuki-coupling of **5** with 4-dimethylaminophenylboronic acid or 4-morpholinophenylboronic acid gave **1d** and **1e** in respective yields of 90 and 93% (Scheme 2b).

The newly prepared quinodimethanes **1d**,**1e** are pale yellow crystalline materials, whose X-ray analyses show that they adopt a folded geometry (Figures 1a and 1b) as in the cases of symmetrically substituted derivatives (**1a**-**1c**).[22] The central hexagon is deformed into a deeply folded boat-form (dihedral angle of about 40°, Table 1).

Upon treatment of **1d**,**1e** with two equivalents of (4-$BrC_6H_4)_3N^{+\bullet}SbCl_6^-$, the corresponding dications **1d**$^{2+}$,**1e**$^{2+}$ were generated and isolated as stable purple $SbCl_6^-$ salts quantitatively in both cases. According to the X-ray analyses (Figures 1c and 1d), both dications adopt a nearly perpendicular geometry (twisting angle of more than 75°, Table 1), which is similar to those of symmetric dications **1a**$^{2+}$-**1c**$^{2+}$. In this way, electronic unsymmetry of aryl substitution does not affect the intrinsic geometrical features of **1** and **1**$^{2+}$.

As detailed later, DFT calculations well reproduced the folded geometry for neutral **1d**,**1e** as well as the twisted geometry for dications **1d**$^{2+}$,**1e**$^{2+}$ (Table 1, Figure S1). It was also confirmed that **1d**$^{2+}$($SbCl_6^-$)$_2$ and **1e**$^{2+}$($SbCl_6^-$)$_2$ could be converted to neutral **1d** and **1e** quantitatively upon reduction with Zn powder in MeCN.

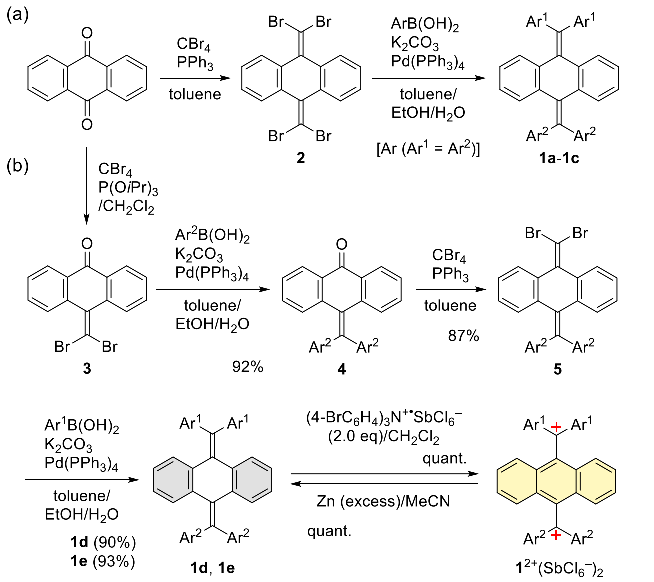

Scheme 2. (a) Preparation of symmetric derivatives **1a**-**1c**. (b) Preparation and redox interconversion of unsymmetrically substituted derivatives **1d**/**1d**$^{2+}$($SbCl_6^-$)$_2$ and **1e**/**1e**$^{2+}$($SbCl_6^-$)$_2$.

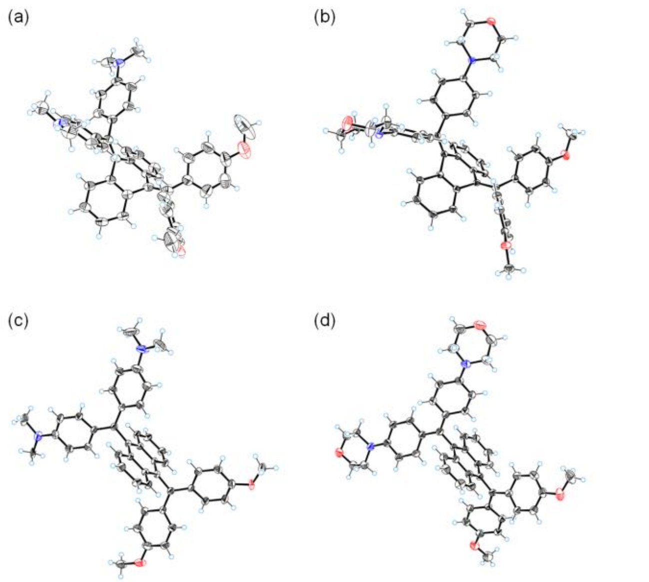

Figure 1. X-ray crystal structures (ORTEP drawings) of (a) **1d**, (b) **1e**, (c) **1d**$^{2+}$($SbCl_6^-$)$_2$, and (d) **1e**$^{2+}$($SbCl_6^-$)$_2$ determined at 150 K. Thermal ellipsoids are shown at the 50% probability level. The counter anions are omitted for clarity for (c) and (d).

Table 1. Structural parameters determined by X-ray analyses and DFT calculations (B3LYP/6-31G*). The calculated values are shown in italics.

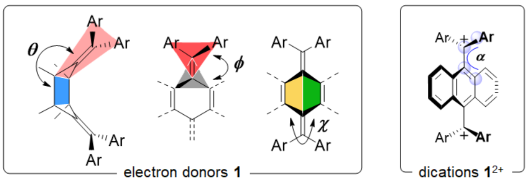

			θ (°)	ϕ (°)	χ (°)	α (°)
1d	Expt.[a]	Ar^1	37.0(3)	8.1(2)	44.1(3)	-
			37.8(3)	6.9(3)	44.6(4)	-
		Ar^2	37.7(3)	6.4(3)		-
			38.0(3)	6.3(2)		-
	Calcd.	*Ar^1*	*37.74*	*10.45*	*44.35*	-
		Ar^2	*38.16*	*8.86*		-
1e	Expt.	Ar^1	34.62(6)	8.37(5)	40.75(7)	-
		Ar^2	32.93(6)	6.44(5)		-
	Calcd.	*Ar^1*	*37.78*	*9.48*	*44.35*	-
		Ar^2	*38.02*	*8.93*		-
1d^{2+}	Expt.[b]	Ar	-	-	-	77.8(7)
	Calcd.	*Ar^1*	-	-	-	*75.8*
		Ar^2	-	-	-	*66.5*
1e^{2+}	Expt.	Ar^1	-	-	-	84.7(5)
		Ar^2	-	-	-	67.3(6)
	Calcd.	*Ar^1*	-	-	-	*76.1*
		Ar^2	-	-	-	*66.3*

[a] Two crystallographically independent molecules. [b] Molecule on the center of symmetry with positional disorder for NMe_2 and OMe groups.

Spectroelectrograms of 1d,1e and 1d^{2+},1e^{2+}.

Neutral **1d**,**1e** exhibit absorption mainly in the UV region whereas strong absorption bands in the visible region are present in the spectra of **1d**$^{2+}$,**1e**$^{2+}$ salt in CH_2Cl_2. There are two major bands (533 and 642 nm for **1d**$^{2+}$, and 533 and 651 nm for **1e**$^{2+}$, respectively), the former of which is similar to that of the symmetric dication **1c**$^{2+}$ (531 nm) with bis(4-methoxyphenyl)methylium units. The latter in the longer-wavelength region is assigned to the band related to bis(dimethylamoinophenyl)methylium or bis(4-morpholinophenyl)methylium units since **1a**$^{2+}$ (628 nm) and **1b**$^{2+}$ (634 nm) exhibit a quite similar absorption band.[22,24]

Upon electrochemical oxidation of **1d** in MeCN containing 0.05 M Bu_4NBF_4 as an electrolyte, drastic color change was observed from nearly colorless to deep purple. The spectroelectrogram showed that the two strong bands at 533 and 642 nm grew simultaneously with the isosbestic points, showing that the spectrum can be accounted for just by considering the presence of **1d** and **1d**$^{2+}$ (Figure 2a). In contrast, upon electrochemical reduction of **1d**$^{2+}$, sequential spectral changes were observed with first disappearance of the band at 533 nm (1st stage) to give blue solution, and then the absorption at 642 nm gradually faded to give the colorless solution (2nd stage) (Figures 2b and 2c).

If we consider that the both stages exhibit isosbestic points, the intermediary blue species should be **1d**$^{+\bullet}$, in which the positive charge is located on the bis(4-dimethylaminophenyl)methylium unit as in **1a**$^{2+}$. Quite similar spectroelectrogram was observed upon electrolyses of **1e** and **1e**$^{2+}$ (Figure 3), showing that the positive charge of **1e**$^{+\bullet}$ is mainly localized on the bis(4-morpholinophenyl)methylium unit.

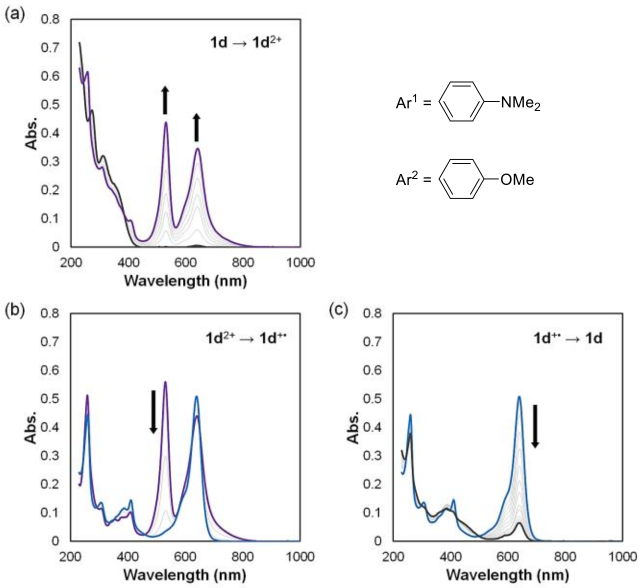

Figure 2. Continuous changes in UV/Vis spectra of (a) **1d** (15 μM) upon constant-current electrochemical oxidation (20 μA, every 4 min) and of (b,c) **1d**$^{2+}$ $(SbCl_6^-)_2$ (4.9 μM) upon constant-current electrochemical reduction (20 μA, every 8 min) in CH_2Cl_2 containing 0.05 M Bu_4NBF_4 as a supporting electrolyte.

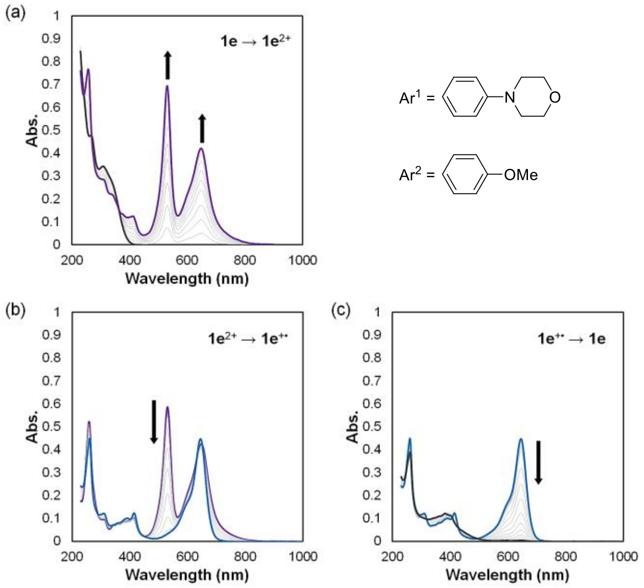

Figure 3. Continuous changes in UV/Vis spectra of (a) **1e** (15 μM) upon constant-current electrochemical oxidation (20 μA, every 4 min) and of (b,c) **1e**$^{2+}$ $(SbCl_6^-)_2$ (5.0 μM) upon constant-current electrochemical reduction (20 μA, every 4 min) in CH_2Cl_2 containing 0.05 M Bu_4NBF_4 as a supporting electrolyte.

In this way, the electrochemical transformation of unsymmetric derivatives occurs in a single stage upon oxidation (from **1d**,**1e** to **1d**$^{2+}$,**1e**$^{2+}$) whereas the reduction is the two-stage process (from **1d**$^{2+}$,**1e**$^{2+}$ to **1d**,**1e** via **1d**$^{+\bullet}$,**1e**$^{+\bullet}$). The observed spectroelectrograms show that the folded quinodimethane **1** undergoes facile 2e-oxidation to twisted **1**$^{2+}$ with the negligible steady-state concentration of **1**$^{+\bullet}$, suggesting that the as-generated **1**$^{+\bullet}$ from **1** undergoes a rapid change into more-easily oxidized species. On the other hand, **1d**$^{2+}$,**1e**$^{2+}$ exhibits the two-stage color change upon electrochemical reduction with the intermediary formation of blue species (**1d**$^{+\bullet}$ and **1e**$^{+\bullet}$).

By considering the twisted geometry of **1**$^{2+}$, it is highly likely that spectroscopically observed **1**$^{+\bullet}$ would adopt a twisted geometry similar to that of **1**$^{2+}$. In this way, the redox process between **1** and **1**$^{2+}$ would involve the geometrical change as shown in Scheme 3, which includes the knowledge that neutral quinodimethane **1** has no contribution from the twisted diradical form **1**$^{\bullet\bullet}$.

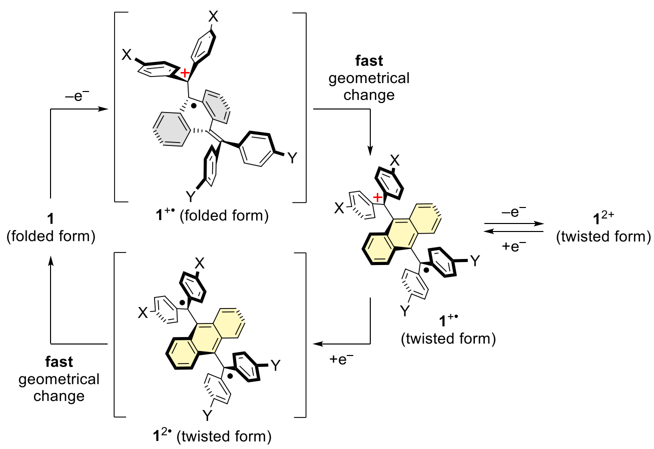

Scheme 3. An estimated mechanism of redox interconversion between **1** and **1**$^{2+}$.

Cyclic voltammograms of 1d,1e and 1d^{2+},1e^{2+}.

By following Scheme 3, the voltammogram would exhibit a 2e-oxidation wave upon conversion of **1d**,**1e** to **1d**$^{2+}$,**1e**$^{2+}$, whereas the two separated 1e-reduction waves would be observed in the reverse cycle for the transformation of **1d**$^{2+}$,**1e**$^{2+}$ to **1d**,**1e** via **1d**$^{+\bullet}$,**1e**$^{+\bullet}$. As shown in Figure 4a, this holds true for the voltammogram of **1d** (1 mM in CH_2Cl_2 at 298 K) with the scan speed of 1 V s^{-1}. Based on the external standard of ferrocene/ferrocenium, oxidation wave of **1d** was confirmed to be a 2e-process, and the oxidation peak at +0.69 V is close to that of **1a** (+0.53 V) with four 4-dimethylaminophenyl groups. The small positive shift in **1d** can be accounted for by the results of DFT calculations that indicated the lower HOMO level of **1d** than of **1a** (-4.59 and –4.42 eV, respectively) (Figure S2).

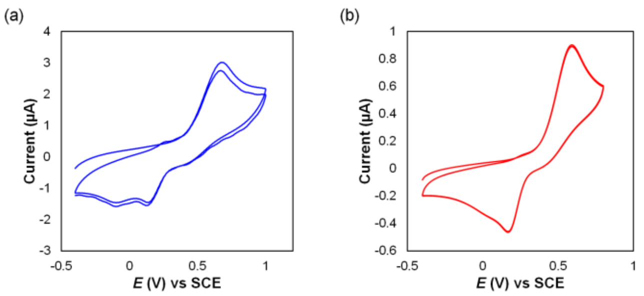

Figure 4. Cyclic voltammograms of **1d** (1 mM) in CH_2Cl_2 containing 0.1 M Bu_4NBF_4 as a supporting electrolyte at 298 K (*E*/V vs SCE, Pt electrodes). Scan rate (a) 1 V s^{-1} and (b) 100 mV s^{-1}.

In the return cycle, there are two peaks corresponding to the reduction of **1d**$^{2+}$ to **1d**$^{+\bullet}$ and the reduction of **1d**$^{+\bullet}$ to **1d** at +0.12 V and –0.19 V vs SCE, respectively. The former value is less positive but still close to the reduction peak of **1c**$^{2+}$ (+0.42 V) with four 4-methoxyphenyl groups, whereas the latter value is similar to that of **1a**$^{2+}$ (–0.33 V). The idea of the first reduction of bis(4-methoxyphenyl)methylium unit in **1d**$^{2+}$ is in accord with the DFT calculation, which predicted that the LUMO of **1d**$^{2+}$ has the coefficients mainly on the bis(4-methoxyphenyl)methylium unit (Figure S2). It should be noted that the reduction wave of **1d**$^{2+}$ at +0.12 V is reversible when the sweep direction was switched just after the first reduction peak (Figure S3a), thus confirming that **1d**$^{+\bullet}$ generated from **1d**$^{2+}$ maintains its twisted geometry. In contrast, the similar reversible wave did not appear when the direction was switched after the second reduction wave, showing that the geometrical change of twisted **1d**$^{2\bullet}$ to folded **1d** is very fast, as expected.

Based on the potential difference (ΔE) of 0.31 V for the two reduction peaks, the intermediary twisted cation radical **1d**$^{+\bullet}$ should be thermodynamically stable (log K = 5.34 where K = [**1d**$^{+\bullet}$]^2/[**1d**$^{2\bullet}$][**1d**$^{2+}$]). However, we found that disproportionation of **1d**$^{+\bullet}$ into **1d**$^{2\bullet}$ and **1d**$^{2+}$ proceeds easily, and the second reduction peak became ambiguous when the voltammogram was measured at 100 mV s^{-1} (Figure 4b). Such observation should be related to the very fast geometrical change from twisted **1d**$^{2\bullet}$ to folded **1d**. Further evidence for the disproportionation process is obtained by measuring the voltammogram at different scan rate, and at different temperatures (Figure S3b,c), showing that the second reduction peak almost disappeared at low scan rate and at higher temperature.

In the voltammograms for the conversion of **1e**$^{2+}$ to **1e** (Figure S4), the second reduction peak is more ambiguous than in the case of **1d**$^{2+}$ to **1d**, since the disproportionation of **1e**$^{+\bullet}$ into **1e**$^{2\bullet}$ and **1e**$^{2+}$ is thermodynamically more favored due to the smaller potential difference for the reduction processes of bis(4-methoxyphenyl)methylium and bis(4-morpholinophenyl)methylium.

Estimated mechanism of the formation of dicationic species.

Thanks to the unsymmetric substitution and the different electronic properties of amino and methoxy groups, the present dications **1d**$^{2+}$,**1e**$^{2+}$ with a twisted geometry undergo stepwise reduction to generate thermodynamically stabilized cation radicals **1d**$^{+\bullet}$,**1e**$^{+\bullet}$. Actually, they were observed as blue species upon electrolyses of CH_2Cl_2 solutions of **1d**$^{2+}$,**1e**$^{2+}$ (10^{-6} M). On the other hand, we also revealed that disproportionation of **1d**$^{+\bullet}$,**1e**$^{+\bullet}$ occurs at higher concentration (10^{-3} M) during the voltammetric analyses, which is facilitated by the rapid conversion of twisted diradicals **1d**$^{2\bullet}$,**1e**$^{2\bullet}$ to folded quinodimethanes **1d**,**1e**.

If we consider that the hypothetical dication diradical **II**$^{2+2\bullet}$ consists of two units of **1**$^{+\bullet}$ which are confined in a proximity, **II**$^{2+2\bullet}$ should undergo intramolecular disproportionation to give another dication diradical **III**$^{2+2\bullet}$ (Scheme 4). Because of the rapid conversion of geometry from twisted form (**1**$^{2\bullet}$) to folded form (**1**), **III**$^{2+2\bullet}$ would be easily transformed to **I**$^{2+}$ with a pentacenequinodimethane skeleton.

Once **I**$^{2+}$ is formed, the oxidation potential of its quinodimethane unit is more positive than that of the diradical unit in **III**$^{2+2\bullet}$, and thus intramolecular electron transfer in **I**$^{2+}$ to form **II**$^{2+2\bullet}$ is energetically disfavored. In this way, we could now clarify the reason why the charge-localized dication with the anthracene core (**I**$^{2+}$) was observed and isolated,[21] while **II**$^{2+2\bullet}$ was not discovered at all.

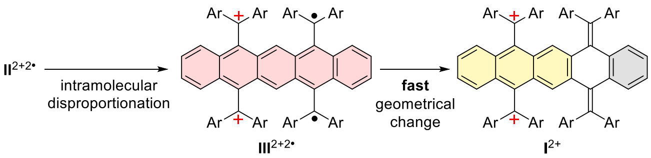

Scheme 4. An estimated mechanism of intramolecular disproportionation from **II**$^{2+2\bullet}$ to **I**$^{2+}$.

Conclusion

In this study, we have succeeded in generating the cation radical (**1**$^{+\bullet}$) of tetraarylanthraquinodimethane, by endowing thermodynamic stability through electronic unsymmetry in the substitution pattern. Thus, for the two derivatives of **1d**$^{2+}$,**1e**$^{2+}$ with both of amino and methoxy groups, the reduction proceeds in a stepwise manner via **1d**$^{+\bullet}$,**1e**$^{+\bullet}$, while maintaining their twisted geometry. The electrochemically generated **1d**$^{2\bullet}$,**1e**$^{2\bullet}$ undergo rapid geometrical change to neutral quinodimethanes **1d**,**1e**, which can be converted back to dications **1d**$^{2+}$,**1e**$^{2+}$ at the higher potential with 2e-transfer. In this way, **1d**$^{+\bullet}$,**1e**$^{+\bullet}$ are the important intermediates of tricolor electrochromism with hysteretic color change of colorless (**1d**,**1e**) -> purple (**1d**$^{2+}$,**1e**$^{2+}$) -> blue (**1d**$^{+\bullet}$,**1e**$^{+\bullet}$) -> colorless (**1d**,**1e**).

At the same time, this work proves that geometrical change of twisted-form **1**$^{2+}$ to folded-form **1** facilitates the disproportionation of **1**$^{+\bullet}$ to **1**$^{2\bullet}$ and **1**$^{2+}$, which rationalize the presence of peculiar dicationic species, whose formation cannot be expected based on the general view for stabilizing the charged organic ions by delocalization and aromatization. The findings obtained in this study would be useful for designing novel oligocationic species, which are generated accompanying geometrical changes.

Experimental Section

All reactions were carried out under an argon atmosphere. All commercially available compounds were used without further purification. Dry MeCN was obtained by distillation from CaH_2 prior to use. Column chromatography was performed on silica gel 60N (KANTO KAGAKU, spherical neutral) of particle size 40-50 µm or Wakogel® 60N (neutral) of particle size 38-100 µm. ^{1}H and ^{13}C NMR spectra were recorded on a BRUKER Ascend™ 400 (^{1}H/400 MHz and ^{13}C/100MHz) spectrometer. IR spectra were measured on a Shimadzu IRAffinity-1S spectrophotometer using the attenuated total reflection (ATR) mode. Mass spectra were recorded on a JMS-T100GCV spectrometer in FD mode by Dr. Eri Fukushi and Mr. Yusuke Takata (GS-MS & NMR Laboratory, Research Faculty of Agriculture, Hokkaido University). Melting points were measured on a Yamato MP-21 and are uncorrected. UV/Vis spectra were recorded on a Hitachi U-2910 spectrophotometer. Redox potentials (E^{ox} and E^{red}) were measured on a BAS ALS-600A by cyclic voltammetry in dry CH_2Cl_2 containing 0.1 M Bu_4NBF_4 as a supporting electrolyte. All of the values shown in the text are in E/V vs. SCE measured at the scan rate of 100 mVs^{-1}. Pt electrodes were used as the working (disk) and counter electrodes. The working electrode was polished using a water suspension of aluminum oxide (0.05 µm) before use. DFT calculations were performed with the Gaussian 16W program package.[26] The geometries of the compounds were optimized by using the B3LYP method in combination with the 6-31G* basis set unless otherwise indicated.

Preparation of 10-bis(4-methoxyphenyl)methylene-9-anthrone (4): A mixture of 10-dibromomethylene-9-anthrone **3** (3.77 g, 10.4 mmol), 4-methoxyphenylboronic acid (4.72 g, 31.0 mmol), K_2CO_3 (5.72 g, 41.4 mmol) and $Pd(PPh_3)_4$ (597 mg, 517 mmol) in toluene (100 mL), EtOH (10 mL), and H_2O (10 mL) was refluxed for 21 h. After cooling to 25 ºC, the mixture was diluted with water and extracted with CH_2Cl_2 three times. The combined organic layers were washed with water and brine, and dried over anhydrous Na_2SO_4. After filtration, the solvent was concentrated under reduced pressure. The crude product was purified by column chromatography on silica gel (hexane/CH_2Cl_2 = 3) to give **4** (3.99 g) as a yellow solid in 92% yield. The spectra data were identical to those in the literature.[27]

Preparation of 11,11-dibromo-12,12-bis(4-methoxyphenyl)-9,10-anthraquinodimethane (5): A mixture of CBr_4 (2.16 g, 6.50 mmol) and PPh_3 (3.41 g, 13.0 mmol) in dry toluene (10 mL) was stirred at 26 ºC for 1 h. To the suspension was added **4** (800 mg, 1.91 mmol), and the mixture was refluxed for 23 h. After cooling to 26 ºC, the reaction mixture was diluted with water. Then, the mixture was extracted with CH_2Cl_2 three times. The combined organic layers were washed with water and brine, and dried over anhydrous Na_2SO_4. After filtration, the solvent was concentrated under reduced pressure. The crude product was purified by column chromatography on silica gel (hexane/EtOAc = 15) to give **5** (959 mg) as a white solid in 87% yield.
Mp: 208-209 ºC; ^{1}H NMR (400 MHz, $CDCl_3$): δ/ppm 7.77 (2H, dd, J =1.2, 7.7 Hz), 7.18 (4H, d, J = 8.7 Hz), 7.10 (2H, dt, J = 1.2, 7.7 Hz), 7.02 (2H, dd, J =1.2, 7.7 Hz), 6.91 (2H, dt, J = 1.2, 7.7 Hz), 6.78 (4H, d, J = 8.7 Hz), 3.75 (6H, s); ^{13}C NMR (100 MHz, $CDCl_3$): δ/ppm 158.36, 141.19, 140.24, 137.50, 136.72, 134.62, 133.76, 130.77, 128.31, 127.06, 126.66, 125.21, 113.68, 88.26, 55.18; IR (ATR) : ν/cm^{-1} 3054, 2995, 2955, 2929, 2906, 2833, 1600, 1570, 1506, 1451, 1439, 1288, 1243, 1172, 1106, 1034, 887, 829, 789, 782, 761, 753, 675, 634, 619, 607, 588, 552, 447; LR-MS(FD) m/z (%): 576.91 (18), 575.90 (53), 574.91 (33), 573.91 (bp), 572.91 (17), 571.91 (M^+, 50); HR-MS (FD) Calcd. for $C_{30}H_{22}O_2Br_2$: 571.99869; Found: 571.99866.

Preparation of 11,11-bis[4-(*N*,*N*-dimethylamino)phenyl]-12,12-bis(4-methoxyphenyl)-9,10-anthraquinodimethane (1d): A mixture of **5** (1.00 g, 1.74 mmol), 4-(*N*,*N*-dimethylamino)phenylboronic acid (1.15 g, 6.97 mmol), K_2CO_3 (963 mg, 6.96 mmol) and $Pd(PPh_3)_4$ (101 mg, 87.0 µmol) in toluene (30 mL), EtOH (3 mL), and H_2O (3 mL) was stirred at reflux for 25 h. After cooling to 25 ºC, the mixture was diluted with water and extracted with EtOAc three times. The combined organic layers were washed with water and brine, and dried over anhydrous Na_2SO_4. After filtration, the solvent was concentrated under reduced pressure. The crude product was purified by column chromatography on silica gel (hexane/EtOAc = 5) to give **1d** (1.03 g) as a yellow-green solid in 90% yield.
Mp: 242-243 ºC; ^{1}H NMR (400 MHz, $CDCl_3$): δ/ppm 7.27 (4H, d, J = 8.6 Hz), 7.18 (4H, d, J = 8.6 Hz), 7.10 (2H, dd, J = 1.7, 6.7 Hz), 7.00 (2H, dd, J = 1.7, 6.7 Hz), 6.80 (4H, d, J = 8.6Hz), 6.76-6.69 (4H, m), 6.62 (4H, d, J = 8.6 Hz), 3.78 (6H, s), 2.91 (12H, s); ^{13}C NMR (100 MHz, $CDCl_3$): δ/ppm 158.11, 149.01, 139.99, 138.89, 138.28, 138.15, 135.68, 135.46, 133.72, 131.36, 130.92, 130.69, 128.03, 127.74, 124.91, 124.59, 113.55, 112.12, 55.19, 40.58; IR (ATR): ν/cm^{-1} 3087, 3062, 3027, 2995, 2948, 2930, 2896, 2856, 2833, 2799, 1604, 1505, 1442, 1344, 1286, 1240, 1189, 1170, 1032, 946, 843, 805, 769, 756, 653, 579, 551; LR-MS(FD) m/z (%): 656.27 (16), 655.27 (54), 654.27 (M^+, bp), 327.63 (9), 327.13 (M^{2+}, 18); HR-MS (FD) Calcd. for $C_{46}H_{42}N_2O_2$: 654.32554; Found: 654.32463; UV/Vis (CH_2Cl_2): λ_{max}/nm (ε/M^{-1}cm^{-1}) 313 (21300), 273 (31700).

Preparation of 11,11-bis(4-methoxyphenyl)-12,12-bis(4-morpholinophenyl)-9,10-anthraquinodimethane (1e): A mixture of **5** (466 mg, 0.811 mmol), 4-morpholinophenylboronic acid (504 mg, 2.43 mmol), K_2CO_3 (449 mg, 3.24 mmol) and $Pd(PPh_3)_4$ (47.0 mg, 40.7 µmol) in toluene (20 mL), EtOH (2 mL), and H_2O (2 mL) was refluxed for 24 h. After cooling to 25 ºC, the mixture was diluted with water and extracted with EtOAc three times. The combined organic layers were washed with water and brine, and dried over anhydrous Na_2SO_4. After filtration, the solvent was concentrated under reduced pressure. The crude product was purified by column chromatography on silica gel (hexane/EtOAc = 2) to give **1e** (558 mg) as a yellow solid in 93% yield.
Mp: 201-202 ºC; ^{1}H NMR (400 MHz, $CDCl_3$): δ/ppm 7.26 (4H, d, J = 8.7 Hz), 7.24 (4H, d, J = 8.7 Hz), 7.05-6.99 (4H, m), 6.80 (4H, d, J = 8.7 Hz), 6.80 (4H, d, J = 8.7 Hz), 6.74-6.71 (4H, m), 3.84 (8H, t, J = 4.8 Hz), 3.78 (6H, s), 3.14 (8H, t, J = 4.8 Hz) ; ^{13}C NMR (100 MHz, $CDCl_3$): δ/ppm 158.19, 149.56, 139.04, 138.63, 138.36, 138.16, 135.40, 135.30, 134.85, 134.41, 130.87, 130.66, 127.95, 127.86, 125.00, 124.87, 115.10, 113.59, 66.93, 55.21, 49.18; IR (ATR): ν/cm^{-1} 3026, 2994, 2951, 2912, 2888, 2833, 2822, 1603, 1506, 1449, 1380, 1336, 1283, 1172, 1119, 1026, 924, 846, 822, 768, 726, 646, 623, 606, 594; LR-MS(FD) m/z (%): 740.31 (20), 739.30 (59), 738.30 (M^+, bp), 370.15 (10), 369.65 (31), 369.15 (M^{2+}, 53); HR-MS (FD) Calcd. for $C_{50}H_{46}N_2O_4$: 738.34660; Found: 738.34576; UV/Vis (CH_2Cl_2): λ_{max}/nm (ε/M^{-1}cm^{-1}) 309 (23300), 268 (33400).

Preparation of anthracene-9-yl-bis(4-methoxyphenyl)methylium-10-yl-bis[4-(*N*,*N*-dimethylamino)phenyl]methylium bis(hexachloroantimonate) [$1d^{2+}(SbCl_6^-)_2$]: To a solution of **1d** (131 mg, 200 µmol) in dry CH_2Cl_2 (10 mL) was added tris(4-bromophenyl)aminium hexachloroantimonate (327 mg, 400 µmol), and the mixture was stirred at 25 ºC for 30 min. The addition of dry ether led to precipitation of the dication salt. The precipitates were washed with dry ether three times and collected by filtration to give **1d**$^{2+}(SbCl_6^-)_2$ (253 mg) as a dark-green powder in 96% yield.
Mp: 167-169 ºC (decomp.); ^{1}H NMR (400 MHz, CD_3CN): δ/ppm 7.90 (4H, br-d, J = 9.3 Hz), 7.72 (2H, dd, J = 2.2, 6.5 Hz), 7.55 (4H, d, J = 8.8 Hz), 7.46-7.37 (6H, m), 7.31 (4H, d, J = 8.8 Hz), 6.93 (4H, d, J = 9.3 Hz), 4.13 (6H, s), 3.28 (12H, s); ^{13}C NMR (100 MHz, CD_3CN): δ/ppm 192.75, 175.08, 170.27, 158.08, 145.24, 140.81, 140.22, 135.92, 132.52, 131.12, 129.52, 128.91, 128.61, 127.55, 127.29, 119.16, 115.59, 79.17, 58.94, 41.60; IR (ATR, KBr pellet) : ν/cm^{-1} 3199, 3098, 3075, 3017, 2979, 2933, 2860, 2846, 2810, 2697, 2672, 2939, 1618, 1607, 1574, 1354, 1273, 1149, 1001, 937,

909, 845, 827, 726, 596, 522; UV/Vis (CH_2Cl_2): λ_{max}/nm (ε/$M^{-1}cm^{-1}$) 642 (90500), 533 (114000), 410 (21100), 309 (22900), 259 (99400).

Preparation of anthracene-9-yl-bis(4-methoxyphenyl)methylium-10-yl-bis(4-morpholinophenyl)methylium bis(hexachloroantimonate) [$1e^{2+}(SbCl_6^-)_2$]: To a solution of **1e** (147 mg, 200 μmol) in dry CH_2Cl_2 (5.0 mL) was added tris(4-bromophenyl)aminium hexachloroantimonate (326 mg, 399 μmol), and the mixture was stirred at 25 ºC for 30 min. The addition of dry ether led to precipitation of the dication salt. The precipitates were washed with dry ether three times and collected by filtration to give **1e**$^{2+}(SbCl_6^-)_2$ (253 mg) as a dark-green powder in 96% yield.

Mp: 170-172 ºC (decomp.); ^{1}H NMR (400 MHz, CD_3CN): δ/ppm 7.90 (4H, br-d, J = 8.8 Hz), 7.72 (2H, dd, J =1.8, 6.7 Hz), 7.58 (4H, d, J = 9.5 Hz), 7.50-7.40 (6H, m), 7.31 (4H, d, J = 8.8 Hz), 7.06 (4H, d, J = 9.5 Hz), 4.14 (6H, s), 3.80 (8H, t, J = 4.5 Hz), 3.72 (8H, t, J = 4.5 Hz); ^{13}C NMR (100 MHz, CD_3CN): δ/ppm 192.63, 175.11, 170.59, 157.75, 145.26, 140.65, 140.44, 136.41, 135.90, 132.50, 131.11, 130.05, 129.55, 128.72, 127.49, 127.32, 119.17, 116.01, 67.05, 58.95, 48.65; IR (ATR, KBr pellet) : ν/cm^{-1} 3076, 2971, 2929, 2901, 2860, 2845, 1576, 1374, 1280, 1239, 1182, 1154, 1130, 1111, 1032, 1005, 926, 910, 844, 825, 595, 542, 515; UV/Vis (CH_2Cl_2): λ_{max}/nm (ε/$M^{-1}cm^{-1}$) 651 (87400), 533 (116000), 415 (20100), 313 (19700), 259 (99800)

Reduction of dication salt $1d^{2+}(SbCl_6^-)_2$ to 1d: To a solution of **1d**$^{2+}(SbCl_6^-)_2$ (70.1 mg, 53.0 μmol) in dry CH_3CN (10 mL) was added activated zinc powder (346 mg, 5.30 mmol). The mixture was stirred at 25 ºC for 30 min, and then diluted with water. The whole mixture was extracted with EtOAc three times. The combined organic layers were washed with water and brine, and dried over anhydrous Na_2SO_4. After filtration through silica gel, the solvent was concentrated under reduced pressure to give **1d** (33.7 mg) as a yellow-green solid in 97% yield.

Reduction of dication salt $1e^{2+}(SbCl_6^-)_2$ to 1e: To a solution of **1e**$^{2+}(SbCl_6^-)_2$ (249 mg, 177 μmol) in dry CH_3CN (20 mL) was added activated zinc powder (1.16 g, 17.7 mmol). The mixture was stirred at 25 ºC for 30 min, and then diluted with water. The whole mixture was extracted with EtOAc three times. The combined organic layers were washed with water and brine, and dried over anhydrous Na_2SO_4. After filtration through silica gel, the solvent was concentrated under reduced pressure to give **1e** (124 mg) as a yellow-green solid in 95% yield.

X-ray analyses: A suitable crystal was selected and measured on a Rigaku XtaLAB Synergy (Cu-Kα radiation, λ = 1.54184 Å) with HyPix diffractometer. The crystal was kept at 150 K during data collection. Using Olex2,[28] the structure was solved with the SHELXT[29] structure solution program using Intrinsic Phasing and refined with the SHELXL[30] refinement package using Least Squares minimization.

*Crystal data of **5***

Crystals were obtained by recrystallization from $CHCl_3$/hexane. MF: $C_{30}H_{22}O_2Br_2$, FW: 574.29, colorless plate, 0.60 × 0.40 × 0.10 mm^3, monoclinic $P2_1/n$, a = 11.68389(15) Å, b = 17.28107(19) Å, c = 12.20309(16) Å, β = 90.6249(11)º, V = 2463.78(5) Å^3, ρ (Z = 4) = 1.548 g cm^{-3}. A total 16726 reflections were measured at T = 150 K. Numerical absorption correction was applied (μ = 4.370 mm^{-1}). The final R_1 and wR_2 values are 0.1033 (I > 2σI) and 0.2831 (all data) for 5082 reflections and 309 parameters. Estimated standard deviations are 0.004-0.007 Å for bond lengths and 0.2-0.4º for bond angles. CCDC 2204203

*Crystal data of **1d***

Crystals were obtained by recrystallization from $CHCl_3$/hexane. MF: $C_{46}H_{42}N_2O_2$, FW: 654.81, colorless plate, 0.40 × 0.10 × 0.03 mm^3, triclinic P1, a = 10.9988(3) Å, b = 11.5100(3) Å, c = 16.0156(5) Å, α = 101.866(2)º, β = 98.345(2)º, γ = 108.358(2)º, V = 1834.49(9) Å^3, ρ (Z = 2) = 1.185 g cm^{-3}. A total 21758 reflections were measured at T = 150 K. Numerical absorption correction was applied (μ = 0.558 mm^{-1}). The final R_1 and wR_2 values are 0.0743 (I > 2σI) and 0.2245 (all data) for 8859 reflections and 912 parameters Estimated standard deviations are 0.006-0.02 Å for bond lengths and 0.4-1.0º for bond angles. CCDC 2204204

*Crystal data of **1e***

Crystals were obtained by recrystallization from benzene/hexane. MF: $C_{50}H_{46}N_2O_4 \cdot (C_6H_6)_2$, FW: 895.10, colorless block, 0.30 × 0.20 × 0.20 mm^3, triclinic P1bar, a = 9.83257(15) Å, b = 13.5240(3) Å, c = 19.0341(3) Å, α = 88.4190(14)º, β = 82.5164(13)º, γ = 75.3361(15)º, V = 2427.73(7) Å^3, ρ (Z = 2) = 1.224 g cm^{-3}. A total 28451 reflections were measured at T = 150 K. Numerical absorption correction was applied (μ = 0.591 mm^{-1}). The final R_1 and wR_2 values are 0.0400 (I > 2σI) and 0.1088 (all data) for 9813 reflections and 615 parameters Estimated standard deviations are 0.0013-0.003 Å for bond lengths and 0.09-0.15º for bond angles. CCDC 2204205

*Crystal data of **1d**$^{2+}(SbCl_6^-)_2$*

Crystals were obtained by recrystallization from dry CH_2Cl_2/ether. MF: $C_{46}H_{42}N_2O_2Cl_{12}Sb_2$, FW: 1323.71, purple plate, 0.20 × 0.05 × 0.02 mm^3, triclinic P1bar, a = 8.8073(3) Å, b = 11.1037(4) Å, c = 14.7519(5) Å, α = 99.878(3)º, β = 100.737(3)º, γ = 107.231(3)º, V = 1313.66(9) Å^3, ρ (Z = 1) = 1.673 g cm^{-3}. A total 13688 reflections were measured at T = 150 K. Numerical absorption correction was applied (μ = 14.083 mm^{-1}). The final R_1 and wR_2 values are 0.0560 (I > 2σI) and 0.1521 (all data) for 5261 reflections and 343 parameters Estimated standard deviations are 0.0013-0.08 Å for bond lengths and 0.05-5º for bond angles. CCDC 2204206

*Crystal data of **1e**$^{2+}(SbCl_6^-)_2$*

Crystals were obtained by recrystallization from dry MeCN/ether. MF: $C_{50}H_{46}N_2O_4Cl_{12}Sb_2$, FW: 1407.79, purple plate, 0.20 × 0.15 × 0.01 mm^3, triclinic P1bar, a = 9.7022(2) Å, b = 16.9382(3) Å, c = 17.37784(16) Å, α = 87.7791(12)º, β = 87.1181(14)º, γ = 78.1293(17)º, V = 2790.05(9) Å^3, ρ (Z = 2) = 1.676 g cm^{-3}. A total 36547 reflections were measured at T = 150 K. Numerical absorption correction was applied (μ = 13.331 mm^{-1}). The final R_1 and wR_2 values are 0.0576 (I > 2σI) and 0.1655 (all data) for 11409 reflections and 633 parameters Estimated standard deviations are 0.0013-0.009 Å for bond lengths and 0.05-0.6º for bond angles. CCDC 2204207

Acknowledgements

We thank Grant-in-Aid from MEXT and JSPS (Nos. 20H02719 and 20K21184 to TS, and 21H01912 and 21H05468 to YI), and JSPS Grant-in-Aid for Research Fellows (Nos. 20J20972 to KS and 22J20578 to TH), Japan. This work was also supported by the Research Program of "Five-star Alliance" in "NJRC Mater. & Dev." MEXT. YI acknowledges Toyota Riken Scholar, the Foundation for the Promotion of Ion Engineering, and the 2020 DIC Award in Synthetic Organic Chemistry, Japan.

Keywords: Redox System • Quinodimethanes • Cations • Radicals • Electrochromism

[1] K. Deuchert, S. Hünig, *Angew. Chem. Int. Ed. Engl.* **1978**, *17*, 875–886.
[2] T. Nishinaga, *Organic Redox Systems*, John Wiley & Sons, Inc, Hoboken, NJ, **2015**.
[3] J. Shukla, V. P. Singh, P. Mukhopadhyay, *ChemistryOpen* **2020**, *9*, 304–324.
[4] V. V. Sentyurin, O. A. Levitskiy, T. V. Magdesieva, *Curr. Opin. Electrochem.* **2020**, *24*, 15–23.
[5] T. Harimoto, Y. Ishigaki, *ChemPlusChem* **2022**, *87*, e202200013.
[6] T. Kubo, *Chem. Rec.* **2015**, *15*, 218–232.
[7] G. E. Rudebusch, G. L. Espejo, J. L. Zafra, M. Peña-Alvarez, S. N. Spisak, K. Fukuda, Z. Wei, M. Nakano, M. A. Petrukhina, J. Casado, M. M. Haley, *J. Am. Chem. Soc.* **2016**, *138*, 12648–12654.
[8] M. Ueda, T. Shirahata, Y. Misaki, *ChemistrySelect* **2017**, *2*, 3490–3495.
[9] P. W. Antoni, M. M. Hansmann, *J. Am. Chem. Soc.* **2018**, *140*, 14823–14835.

[10] C. Zhu, X. Ji, D. You, T. L. Chen, A. U. Mu, K. P. Barker, L. M. Klivansky, Y. Liu, L. Fang, *J. Am. Chem. Soc.* **2018**, *140*, 18173–18182.
[11] K. Oki, M. Takase, S. Mori, H. Uno, *J. Am. Chem. Soc.* **2019**, *141*, 16255–16259.
[12] Y. Ni, T. Y. Gopalakrishna, H. Phan, T. Kim, T. S. Herng, Y. Han, T. Tao, J. Ding, D. Kim, J. Wu, *Nat. Chem.* **2020**, *12*, 242–248.
[13] Y. K. Loh, P. Vasko, C. McManus, A. Heilmann, W. K. Myers, S. Aldridge, *Nat. Commun.* **2021**, *12*, 7052.
[14] P. W. Antoni, C. Golz, M. M. Hansmann, *Angew. Chem. Int. Ed.* **2022**, *61*, e202203064.
[15] R. Kumar, P. J. Chmielewski, T. Lis, D. Volkmer, M. Stępień, *Angew. Chem. Int. Ed.* **2022**, e202207486.
[16] S. Patai, Z. Rappoport, Eds. , *The Quinonoid Compounds: Vol. 1 (1988)*, John Wiley & Sons, Inc., Chichester, UK, **1988**.
[17] S. Patai, Z. Rappoport, Eds. , *The Quinonoid Compounds: Vol. 2 (1988)*, John Wiley & Sons, Inc., Chichester, UK, **1988**.
[18] Y. Ishigaki, K. Sugawara, T. Tadokoro, Y. Hayashi, T. Harimoto, T. Suzuki, *Chem. Commun.* **2021**, *57*, 7201–7214.
[19] T. Hamura, R. Nakayama, K. Hanada, Y. Sakano, R. Katoono, K. Fujiwara, T. Suzuki, *Chem. Lett.* **2013**, *42*, 1244–1246.
[20] K. Kobayashi, Y. Mazaki, *J. Synth. Org. Chem. Jpn.* **1988**, *46*, 638–653.
[21] Y. Ishigaki, T. Harimoto, K. Sugawara, T. Suzuki, *J. Am. Chem. Soc.* **2021**, *143*, 3306–3311.
[22] Y. Ishigaki, K. Sugawara, M. Yoshida, M. Kato, T. Suzuki, *Bull. Chem. Soc. Jpn.* **2019**, *92*, 1211–1217.
[23] Y. Ishigaki, T. Hashimoto, K. Sugawara, S. Suzuki, T. Suzuki, *Angew. Chem. Int. Ed.* **2020**, *59*, 6581–6584.
[24] Y. Sakano, R. Katoono, K. Fujiwara, T. Suzuki, *Chem. Lett.* **2014**, *43*, 1143–1145.
[25] T. Nishiuchi, S. Aibara, T. Kubo, *Angew. Chem. Int. Ed.* **2018**, *57*, 16516–16519.
[26] M. J. Frisch, G. W. Trucks, H. B. Schlegel, G. E. Scuseria, M. A. Robb, J. R. Cheeseman, G. Scalmani, V. Barone, G. A. Petersson, X. Nakatsuji, H.; Li, M. Caricato, A. V. Marenich, J. Bloino, B. G. Janesko, R. Gomperts, B. Mennucci, H. P. Hratchian, J. V. Ortiz, A. F. Izmaylov, J. L. Sonnenberg, D. Williams-Young, F. Ding, F. Lipparini, F. Egidi, J. Goings, B. Peng, A. Petrone, T. Henderson, D. Ranasinghe, V. G. Zakrzewski, J. Gao, N. Rega, G. Zheng, W. Liang, M. Hada, M. Ehara, K. Toyota, R. Fukuda, J. Hasegawa, M. Ishida, T. Nakajima, Y. Honda, O. Kitao, H. Nakai, T. Vreven, K. Throssell, J. A. J. Montgomery, J. E. Peralta, F. Ogliaro, M. J. Bearpark, J. J. Heyd, E. N. Brothers, K. N. Kudin, V. N. Staroverov, T. A. Keith, R. Kobayashi, J. Normand, K. Raghavachari, A. P. Rendell, J. C. Burant, S. S. Iyengar, J. Tomasi, M. Cossi, J. M. Millam, M. Klene, C. Adamo, R. Cammi, J. W. Ochterski, R. L. Martin, K. Morokuma, O. Farkas, J. B. Foresman, D. J. Fox, *Gaussian 16, Revision A.03*, Gaussian, Inc., Wallingford CT, 2016, **n.d.**
[27] A. Schönberg, A. F. A. Ismail, W. Asker, *J. Chem. Soc.* **1946**, 442–446.
[28] O. V. Dolomanov, L. J. Bourhis, R. J. Gildea, J. A. K. Howard, H. Puschmann, *J. Appl. Crystallogr.* **2009**, *42*, 339–341.
[29] G. M. Sheldrick, *Acta Crystallogr. Sect. A Found. Adv.* **2015**, *71*, 3–8.
[30] G. M. Sheldrick, *Acta Crystallogr. Sect. C Struct. Chem.* **2015**, *71*, 3–8.

Entry for the Table of Contents

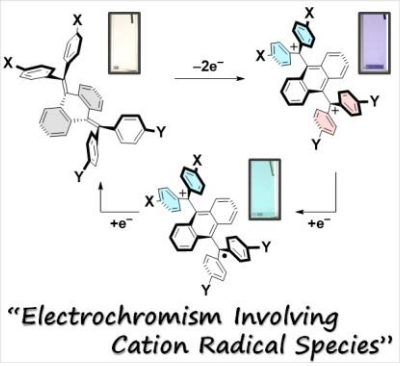

The twisted cation radical is the stable intermediate upon redox interconversion between the folded tetraarylanthraquinodimethane and the twisted dication with an anthracene core attached with two diarylmethylium units. By introducing electronic unsymmetry, the long-lived cation radical can be involved in the electrochromism, which appears only in the reduction step. This tricolor electrochromicity demonstrates a hysteretic pattern of color change.

Institute and/or researcher Twitter usernames: Yusuke Ishigaki (@ysk_isgk); Takanori Suzuki (@Yuuichi_Hokudai)